Fine-particle emissions from solid biofuel combustion studied with single-particle mass spectrometry: Identification of markers for organics, soot, and ash components

Pagels, Joakim; Dutcher, Dabrina D.; Stolzenburg, Mark R.; McMurry, Peter H.; Gaelli, Markus E.; Gross, Deborah S.

Published in:
Journal of Geophysical Research: Atmospheres

DOI:
10.1029/2012JD018389

2013

Document Version:
Publisher's PDF, also known as Version of record

JOURNAL OF GEOPHYSICAL RESEARCH: ATMOSPHERES, VOL. 118, 859–870, doi:10.1029/2012JD018389, 2013

Fine-particle emissions from solid biofuel combustion studied with single-particle mass spectrometry: Identification of markers for organics, soot, and ash components

Joakim Pagels,[1,2] Dabrina D. Dutcher,[1] Mark R. Stolzenburg,[1] Peter H. McMurry,[1] Markus E. Gälli,[3] and Deborah S. Gross[4]

Received 2 July 2012; revised 16 October 2012; accepted 3 November 2012; published 17 January 2013.

[1] The effects of combustion phase and fuel on smoke particle emissions from a wood stove operated with three different wood fuels and from a corn stove were investigated. A single-particle mass spectrometer (aerosol time of flight mass spectrometer (ATOFMS)) was used for time- and size-resolved chemical signatures and a scanning mobility particle sizer (SMPS) was used for online mobility size distributions. Markers of particle phase organics and elemental carbon, $PM_{1.5}$, and CO emissions were strongly reduced for the corn stove compared to the wood stove. This is because the more controlled fuel and air supply in the corn stove result in more complete combustion. NO_x emissions and particle phase phosphates showed the opposite trend. Marker ions and particle types associated with soot and alkali salts such as potassium chloride and potassium sulfates dominated during flaming combustion and were correlated with increased exhaust temperatures and reduced CO emissions. Marker ions of hydrocarbons and oxidized organics as well as a particle cluster type with a strong organic signature were associated with reduced combustion temperature and increased CO levels, observed during start up from cold stove, addition of fuel, and combustion with reduced air supply. Two different particle types were identified in corn experiments when particles were classified according to mobility before they were measured with the ATOFMS. "Less massive" particles contained mostly ash and soot and had vacuum aerodynamic diameters that were nearly independent of mobility diameter. "More massive" particles had aerodynamic diameters that increased linearly with mobility diameter, indicating approximately spherical shapes, and were hypothesized to consist of organics.

Citation: Pagels, J., D. D. Dutcher, M. R. Stolzenburg, P. H. McMurry, M. E. Gälli, and D. S. Gross (2013), Fine-particle emissions from solid biofuel combustion studied with single-particle mass spectrometry: Identification of markers for organics, soot, and ash components, *J. Geophys. Res. Atmos.*, *118*, 859–870, doi:10.1029/2012JD018389.

1. Introduction

[2] Replacement of fossil fuels by biofuels in residential heating can decrease the net emissions of greenhouse gases such as CO_2 to the atmosphere. Biofuels that have been used include wood logs and wood pellets as well as novel crop fuels such as corn. At the same time, smoke emissions from such fuels can lead to air pollution (e.g., $PM_{2.5}$ and PM_{10}) that adversely affects human health [*Naeher et al.*, 2007; *Bolling et al.*, 2009; *Sehlstedt et al.*, 2010]. Particles from solid biomass combustion can be a major contributor to PM2.5 even in larger cities in the winter time [*Favez et al.*, 2009; *Caseiro et al.*, 2009]. Airborne particles also affect global climate [*Intergovernmental Panel on Climate Change*, 2007]. Small-scale combustion systems used for residential heating range from conventional fireplaces and stoves to small residential boilers for single-family houses (smaller than 20 kW).

[3] Particle emission factors from woody biofuels can be relatively high in comparison to other fuels used for energy production [*Bolling et al.*, 2009]. Previous research has focused on particle number and mass emission factors [*Johansson et al.*, 2004] and the particle chemical composition [*Boman et al.*, 2004; *Lillieblad et al.*, 2004; *Wierzbicka et al.*, 2005; *Tissari et al.*, 2008a] averaged over a full combustion cycle. In these studies impactor or filter samplers were used and particle mass and chemical composition was analyzed off-line. Other studies have focused on the organic composition [*Fine et al.*, 2004] or the speciation of inorganic ash compounds [*Wiinikka et al.*, 2007].

All Supporting information may be found in the online version of this article.

[1]Particle Technology Laboratory, Department of Mechanical Engineering, University of Minnesota, Twin Cities, Minneapolis, Minnesota, USA.
[2]Ergonomics and Aerosol Technology, Lund University, Lund, Sweden.
[3]TSI Inc., Shoreview, Minnesota, USA.
[4]Department of Chemistry, Carleton College, Northfield, Minnesota, USA.

Corresponding author: J. Pagels, Ergonomics and Aerosol Technology, Lund University, PO box 118, SE 221 00 Lund, Sweden. (joakim.pagels@design.lth.se)

2169-897X/13/2012JD018389

[4] These studies have shown that the particle emissions from wood combustion systems/appliances during less optimized combustion in small-scale wood combustion are most often dominated by products of incomplete combustion, i.e., organic and elemental carbon (OC and EC). In contrast, during optimized combustion in modern domestic wood pellet combustion systems, the aerosol is often dominated by ash compounds, especially KCl, K_2SO_4 and K_2CO_3 formed via evaporation-condensation and heterogeneous reactions in the gas phase [*Christensen et al*., 1998; *Pagels et al*., 2003] and the total carbon contribution can be lower than 1% [*Londahl et al*., 2008]. The volatilization of ash components during combustion resulting in ash particle emissions increases with increasing combustion temperature [*Wiinikka et al*., 2007], therefore combustion in a state-of-the-art burner may dramatically decrease the emissions of OC and EC but potentially increase the emissions of ash components. Crop fuels have higher ash content than conventional wood fuels [*Tissari*, *et al*., 2008b, *Wolnik et al*., 1985] due to a high concentration of nutrients such as potassium, sulfur, chloride, nitrogen and phosphorus in the fuel. This influences the emission levels, the particle size distribution, and the composition of the particle emissions.

[5] Knowledge about variations in the particle size distribution during the combustion cycle has increased over the last few years [*Tissari et al*., 2008a]. However, little research has been carried out to study the variations in physical and chemical properties of particles emitted through the combustion cycle. *Rissler et al*. [2005] combined highly time-resolved particle size and gas analysis with off-line OC/EC analysis and found a correlation between short-lived CO concentration peaks, increased particle concentrations in the 150–500 nm size range, and increased EC concentrations. However, the detailed time-resolved mixing between ash, organic carbon and elemental carbon remains poorly understood. *Tissari et al*. [2009] divided the combustion cycle into three different phases where separate filter samples were collected and found that the organic emissions increased during the firing phase (start-up). Thus, better knowledge of time-dependent aerosol chemical properties may potentially lead to emission reductions by identifying processes associated with increased emissions of certain chemical components, which can then be addressed.

[6] Over the last 10–15 years, aerosol mass spectrometers (AMS) have been developed for highly time-resolved in situ measurements of the particle chemical composition. *Weimer et al*. [2008] applied a quadrupole aerosol mass spectrometer (Q-AMS; Aerodyne Research) to study the composition of particle emissions from a conventional wood stove. They found an increased concentration of organic carbon (for example, markers of levoglucosan) during the start-up phase of the combustion cycle. With the conventional AMS, only materials that volatilize at 600 °C can be analyzed. Thus, soot and low-volatility ash components such as K_2SO_4 are not detected. *Grieshop et al*. [2009] and *Heringa et al*. [2011] also used AMS techniques to characterize the composition of wood stove emissions, although their studies focused on atmospheric processing of the emissions rather than variations of primary emissions over the combustion cycle. AMS measurements of ambient air have linked concentrations of certain classes of organics to biomass combustion emissions [*Alfarra et al*., 2007].

[7] Although aerosol MS techniques involving laser desorption and ionization [*Gard et al*., 1997] do not allow quantitative measurements of mass concentrations due to the matrix effects and laser inhomogeneities inherent in the ionization process, they provide chemical signatures on a single-particle level for the major particulate emissions types formed during solid biofuel combustion (ash, OC, and EC), and ion intensities and ratios have been shown to scale with off-line techniques in numerous studies [*Pratt and Prather*, 2012]. *Silva et al*. [1999] used an aerosol time of flight mass spectrometer (ATOFMS) to investigate smoke emissions from combustion of wood species commonly found in California. They identified strong peaks from potassium, chloride and sulfate and several organic markers potentially unique to biomass combustion. Several field studies have used ATOFMS to identify particle types that can be associated with emissions from biomass combustion [*Qin and Prather*, 2006; *Moffet et al*., 2008; *Healy et al*., 2010; *McGuire et al*., 2011]. The mass spectra of the biomass particle type has in general been consistent with the source spectra determined by *Silva et al*. [1999], but with overlaid signatures of atmospheric processing. However, to our knowledge there are no single-particle mass spectrometry data that have systematically investigated relationships between variations in particle composition for different fuels and in the combustion phase/efficiency.

[8] In this work, we combined single-particle mass spectrometry with time-resolved measurements of the mobility particle size distribution and particle mass concentration to investigate chemical signatures and emissions from three wood log fuels (oak, pine and birch) and corn, burned in residential wood- and corn-burning stoves. The aim was to investigate the influence of combustion phase and fuel on the emission levels and the particle composition.

2. Methods

2.1. Combustion Appliances

[9] Two different stoves were used for the combustion of the log wood fuels and the corn fuel, respectively. A wood stove (model Lopi "Answer", Travis Industries, WA, USA) with a rated maximum heat output of 20 kW was operated with jack pine, oak and birch logs. All these fuels were locally grown in Minnesota and were dried for at least 6 months prior to the experiments. Each wood combustion experiment involved start-up from a cold stove with a full load of fuel. Fuel was then added once or twice and experiments were conducted until only glowing embers remained. The wood stove was normally operated with the vent for air supply fully open. In this stove type, secondary air is added at the end of the combustion chamber to improve combustion efficiency.

[10] To investigate relationships between combustion conditions and emission characteristics, each wood stove experiment was divided into combustion phases based on the CO and O_2 measurements in the flue gas. Briefly, each combustion cycle started with either "start-up" from a cold stove or "added fuel" on glowing embers. This was followed by a "flaming" phase and each cycle ended with a "burnout" phase. The flaming phase was subdivided into "flaming effective"; "flaming high CO"; and "choked" depending on the CO emission level and setting of the air supply valve. A more

comprehensive description of the combustion experiments and the division of the combustion cycle into different combustion phases is given in the supporting information.

[11] Dried corn kernels were combusted in a corn stove (model "Auburn", St Croix Pellet and Corn Stoves, NE, USA). This corn stove is top fed and the dried corn kernels are added to the combustion region at a controlled rate, similar to modern wood pellet stoves. This allows a significantly enhanced control of the fuel supply compared to batch-wise combustion of wood logs. The corn stove was started using wood pellets, and the fuel was manually switched to corn upon a successful start-up procedure as indicated by CO concentrations below 1000 ppm. The corn stove was operated under essentially steady state combustion conditions at 50% of the 12 kW maximum capacity.

2.2. Sampling and Dilution

[12] Separate sampling probes were used for particle and gas analysis. These were taken from the middle of the flue gas duct at a distance of about 50 cm above the wood stove outlet (flue gas temperatures in this position varied over the combustion cycle in the range of 100–400 °C). In the corn stove, the measurement point was at a position 30 cm downstream of the stove outlet (flue gas temperature ~170 °C).

[13] A schematic of the sampling system is given in Figure 1. The sample was diluted by a factor of 15 with dried particle-free air at ambient temperature after which it flowed through a 2 s residence time chamber. Two additional dilution stages were used to allow ATOFMS measurements at an optimal counting rate. Additional details of the dilution system for particle measurement, and the instrumentation used, are provided in the supporting information.

2.3. Aerosol Characterization

[14] Particles were characterized using an aerosol time-of-flight mass spectrometer (ATOFMS; TSI Inc.) [*Gard et al*., 1997] equipped with an aerodynamic lens (50–500 nm) [*Dutcher et al*., 2011], for single-particle chemical composition analysis. Further descriptions of the ATOFMS operating parameters and data reductions techniques are given in the supporting information. In a few corn emission experiments, a differential mobility analyzer (Long column DMA, TSI Inc.) was used upstream of the ATOFMS for composition and effective density measurements of mobility classified particles [*Park et al*., 2008]. In these cases the ATOFMS measured the vacuum aerodynamic diameter and composition of DMA classified particles of six mobility sizes between 100 and 325 nm. A scanning mobility particle sizer (SMPS) was used to determine the particle size distribution (16–750 nm). The SMPS sampled downstream of the second dilution stage (after the first laminar flow diluter). Each size distribution (5 min resolution) is the average of one up scan and one down scan. A tapered element oscillating microbalance (TEOM, Thermo Scientific) was used to determine the total particulate mass concentration. The upper size cut (1.5 μm) was determined by the cyclone in the sampling system. The instrument was operated at a temperature of 50 °C with a sampling flow rate of 1 L/min.

[15] A flue gas analyzer (CA-Calc 7315, TSI Inc.) sampling undiluted exhaust through a separate sampling line was used to determine the concentration of CO, O_2, NO, NO_2, and the flue gas temperature. A second flue gas analyzer (model AC, ECOM) sampled downstream of the primary dilution stage and allowed online determination of the primary dilution ratio from NO measurements with the two analyzers. Particle and gas emission factors (in units of mg/MJ) were calculated from the measured concentrations according to a mass balance procedure [*van Loo and Koppejan*, 2008]. This used inputs in the form of measured O_2, CO and water vapor (from RH and T measurements after primary dilution) concentration in the flue gas and tabulated values of wood log and corn kernel fuel elemental composition and heating values. This procedure also yielded the CO_2 concentration in the flue gas as output.

3. Results and Discussion

3.1. Emission Factors and Particle Size Distributions

[16] The emission factors of $PM_{1.5}$, CO, and NO_x varied strongly between corn and wood combustion. For corn, the average $PM_{1.5}$, CO, and NO_x emission factors were 30, 130 and 270 mg/MJ, respectively. For wood combustion, the average CO values over full cycles were 1500, 1600 and 2600 mg/MJ for oak, birch and pine respectively. $PM_{1.5}$ was measured over a full cycle for the pine fuel (90 mg/MJ) and NO_x was measured for the birch fuel (90 mg/MJ).

[17] The low CO and $PM_{1.5}$ emissions for the corn stove are similar to those observed from modern wood pellet burners [*Bolling et al*., 2009]. This is due to the controlled

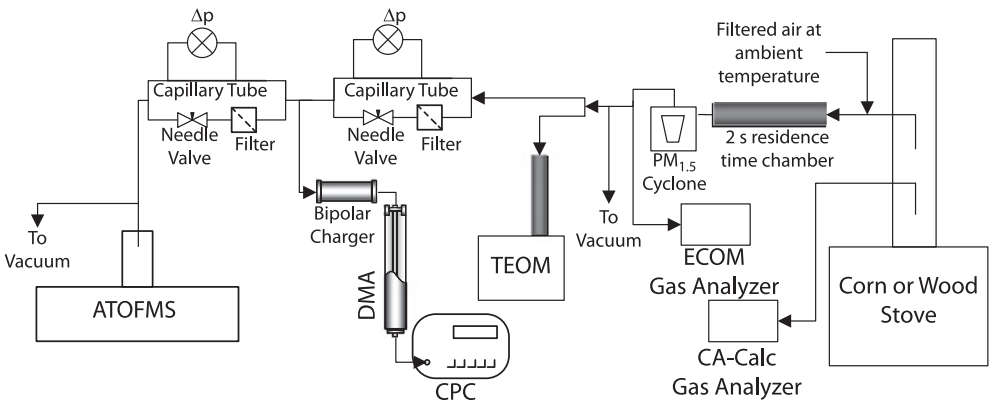

Figure 1. Schematic of the experimental setup, showing the various sampling devices attached to the dilution stages.

fuel supply and mixing of air and fuel, resulting in more complete combustion which reduces emissions of products of incomplete combustion such as organics, elemental carbon and CO. In the wood stove, on the other hand, there will unavoidably be fuel-rich time periods and regions in the combustion zone, resulting in higher PM and CO emissions.

[18] The emission factors from the wood stove are within the lower end of those from conventional wood stoves and within the range of those for modern wood stoves [*Bolling et al*., 2009; *Pettersson et al*., 2011]. The lower emission factors, compared to conventional wood stoves, are partly a result of the fact that secondary air is supplied later in the combustion process which combusts a significant portion of the products of incomplete combustion, thus significantly reducing CO and PM emissions. The largest differences in CO emissions between the wood fuels occurred during the flaming phase. The CO emissions of the hard wood fuels (birch and oak) were more than three times lower than that of the soft wood fuel (pine).

[19] The NO_x emissions showed a reverse trend, with significantly higher emissions for the corn stove. *Tissari et al*., 2008b showed that two crop fuels (oat and rape seeds) generated 4–10 times higher NO_x emissions compared to wood pellets used in the same burner. The increased NO_x emissions were attributed to higher nitrogen content in the fuel; this is likely the explanation for these observations with corn fuel as well.

[20] Average mobility particle size distributions for emissions from the four fuels are shown in Figure 2. There are rather small differences between the three wood fuels, except below about 30 nm (lower emissions from pine) and above 200 nm (lower emissions for oak). The corn emissions have significantly lower concentration of particles above 100 nm, consistent with the low $PM_{1.5}$ mass emission factor for corn combustion. There is evidence that the number distribution for corn emissions increases above 300 nm. The average total number concentrations for the different fuels ranged from 2 to 3×10^8 cm^{-3}, which is within the higher end compared to previously reported values [*Pettersson et al*., 2011, *Tissari et al*., 2008a].

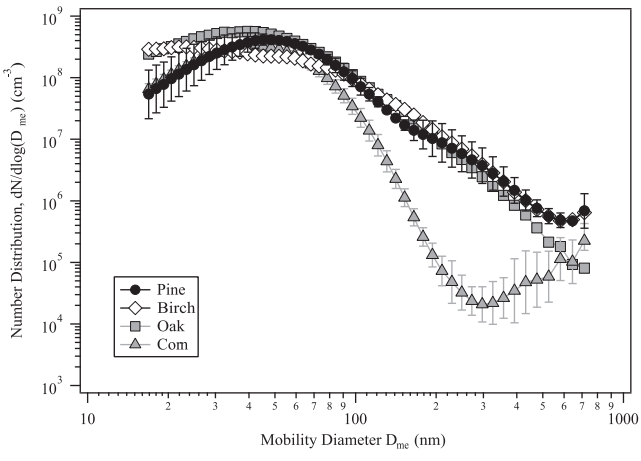

Figure 2. Mobility size distribution averaged over the combustion cycle for each of the fuels. Error bars (±1 standard deviation) based on replicate measurements are shown only for pine and corn for ease of visualization.

[21] Figure 3 shows the mobility size distribution as a function of combustion phase for the wood stove experiments. It can be seen that both the start-up phase and addition of more wood logs generate a higher concentration of particles larger than 100 nm compared to the average of the full cycles. On the other hand, during the flaming effective combustion phase (flaming combustion with a CO concentration below 1000 ppm), significantly more sub-30 nm particles and less particles above about 70 nm are emitted, producing a size distribution with similarities to the distribution observed from the corn stove.

[22] The mobility size distribution could in many cases be described as bimodal with a nucleation mode below 70 nm and a larger accumulation mode. The experiments in this paper focus on the chemistry of particles above about 80–100 nm due to the low detection efficiency of the ATOFMS for smaller sizes. Thus the focus is on the accumulation mode that may dominate the mass concentration but contributes relatively little to the number concentration.

3.2. Influence of Fuel on Marker Ions in Single-Particle Mass Spectra

[23] The mass spectra of particles emitted from the wood and the corn stoves averaged over the full combustion cycle are given in Figure S1. Selected marker ions that varied between fuels are shown in Figure 4. In general, the mass spectra of emissions from the three wood fuels show strong similarities. Major identified peaks associated with inorganic species that were vaporized in the combustion process include $^{39}K^+$, $^{23}Na^+$, $^{113}K_2Cl^+$ and $^{213}K_3SO_4^+$ in the positive spectra and $^{35}Cl^-$, $^{80}SO_3^-$, $^{97}HSO_4^-$ and $^{109}KCl_2^-$ in the negative spectra (and associated isotope peaks). This is expected since potassium chloride and potassium sulfate are well known constituents of emissions from wood combustion [*Pagels et al*., 2003].

[24] The markers for EC: C_n^- (e.g., $^{24}C_2^-$, $^{36}C_3^-$, and $^{48}C_4^-$) are pronounced in the average mass spectra. There are also

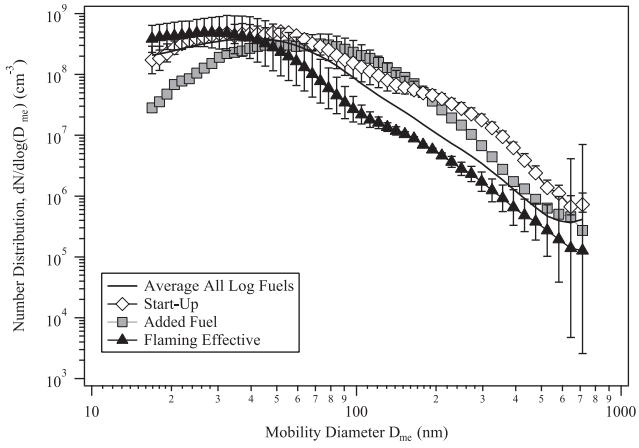

Figure 3. Influence of combustion phase on mobility size distribution. Averages of the three wood fuels for start-up, added fuel, and flaming effective (only oak and birch) are compared to the whole-cycle average. Error bars (±1 standard deviation) based on replicate measurements are shown only for flaming effective and start-up for ease of visualization.

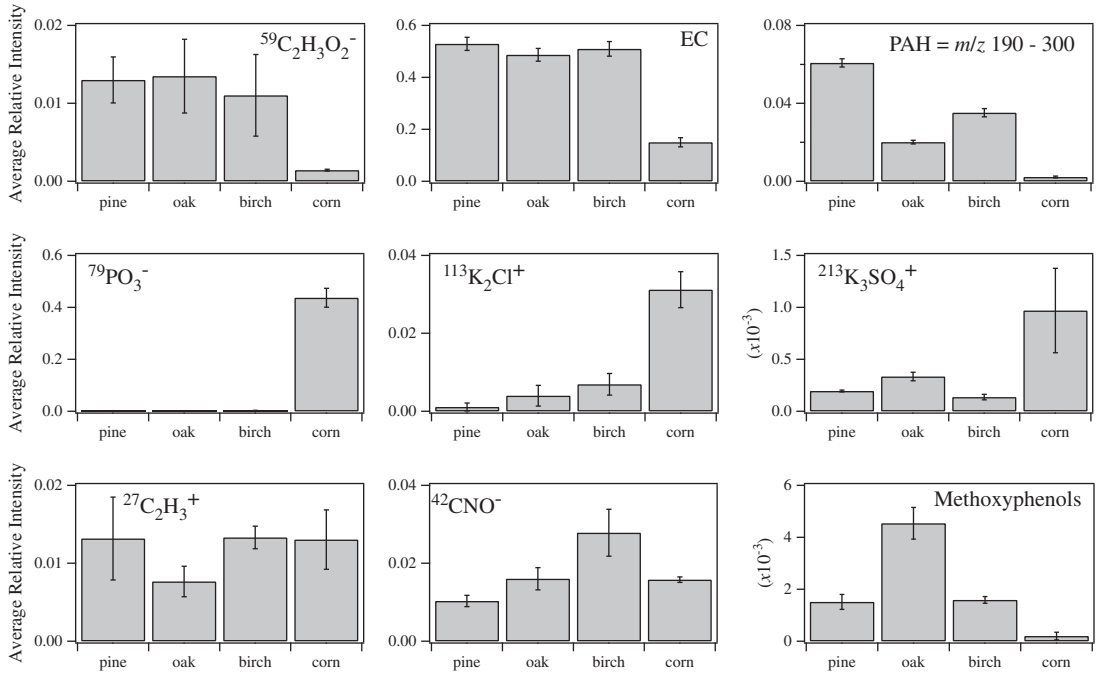

Figure 4. Trends in the average relative peak intensity of (top) markers for oxidized organics, EC, and PAHs, (middle) phosphates, potassium chloride, and potassium sulfate, and (bottom) hydrocarbons, compounds containing both nitrogen and organics, and methoxyphenols as a function of fuel type in ATOFMS mass spectra averaged over the full combustion cycle for each fuel. Error bars represent ±1 standard deviation of replicate measurements.

markers for hydrocarbons (e.g., $^{27}C_2H_3^+$) and oxidized organics (e.g., $^{59}C_2H_3O_2^-$). The peak m/z = -59 is commonly used as a tracer of biomass combustion particles in ambient ATOFMS data, as it is a signature of monosaccharaides such as levoglucosan formed by the pyrolysis of cellulose [*Silva et al*., 1999].

[25] We found high molecular weight peaks in both the positive and negative spectra. Peaks between m/z = 190 and 300 in the positive spectra were approximated to be due to polycyclic aromatic hydrocarbons (PAHs). The strongest peaks at higher m/z in the negative spectra for the wood fuels were m/z = -136, -137, -138 and m/z = -162, -163, -164. In this study, the relative peak areas of these six peaks were summed and used as an indicator of methoxy phenol fragments. In a previous study, -137 and -163 were assigned to deprotonated methyl guaiacol and eugenol fragments [*Qin and Prather*, 2006]. Methoxyphenols originate as pyrolysis products of lignin present in the wood fuels.

[26] A few differences between the mass spectra from the three wood fuels should be noted. The pine experiments show stronger peaks for sodium and high mass positive ions including PAHs, while markers of compounds containing both nitrogen and organics ($^{26}CN^-$, $^{42}CNO^-$) and nitrates ($^{46}NO_2^-$, $^{62}NO_3^-$) are enhanced for oak and birch compared to pine. The highest contribution from methoxyphenols was found for oak.

[27] A much larger difference was found between the wood fuels and the corn fuel, as seen in Figure 4. Markers for inorganic ash components were significantly more pronounced for corn (e.g., $^{113}K_2Cl^+$ and $^{213}K_3SO_4^+$). However, the most striking difference was the strong signature of phosphates ($^{63}PO_2^-$ and $^{79}PO_3^-$). These peaks were of very low intensity for the three wood fuels. The signatures for EC, oxidized organics (e.g., m/z = -59), PAHs and methoxyphenols were weaker for the corn stove compared to the wood stove. Markers for hydrocarbons (e.g., m/z = 27) and fragments containing both carbon and nitrogen (e.g., $^{42}CNO^-$) were comparable in the wood and corn combustion spectra.

[28] Little published information exists about the composition of particle emissions from domestic combustion of corn kernels. However, *Tissari et al*. [2008b] studied emissions from other crop fuels which have some common features with corn. They showed that about 7% of the PM_1 emissions consisted of phosphate ions when rapeseed was combusted in a wood pellet burner; no phosphates were detected when operating the same pellet burner with wood fuels. The concentration of phosphorus is higher in corn compared to typical wood fuels [*Tao et al*., 2012]. Additionally, on a relative basis, the Ca content is substantially lower in corn compared to the wood fuels. Ca has been shown to form calcium phosphates, which effectively traps P in the bottom ash [*Boström et al*., 2012] for most wood fuels. The lower Ca concentration in the corn fuel may allow the formation of Potassium Phosphates that are eventually emitted as fine particles.

3.3. Influence of Combustion Phase on Marker Ions in Single-Particle Mass Spectra

[29] The suite of online techniques used in these experiments allowed us to investigate variations in emission characteristics and levels over the combustion cycles for the inherently transient combustion in the wood stove. Figure 5 shows an example of time–resolved data for the birch combustion experiment. It is clear that adverse combustion conditions identified by elevated CO emissions and

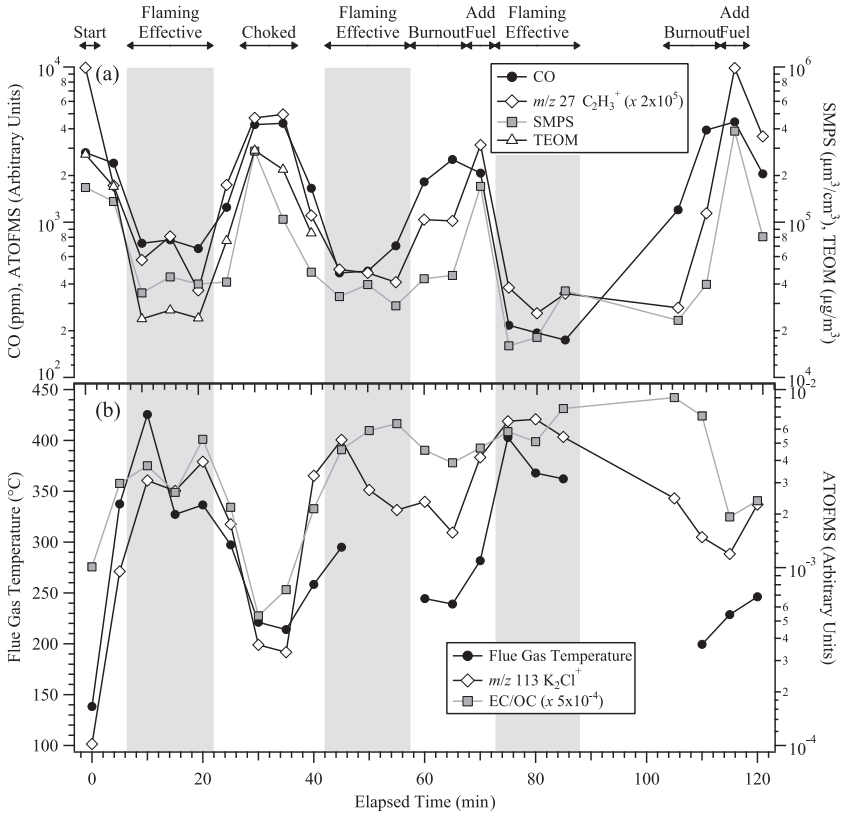

Figure 5. Time dependence of emissions from the birch combustion experiment, including (a) particle mass (TEOM), effective volume (SMPS), a marker peak for hydrocarbons (ATOFMS) and CO and (b) flue gas temperature, and an ash marker peak from ATOFMS. The EC/OC peak ratio estimated from the ATOFMS spectra is also shown in Figure 5b. All ATOFMS data are given as relative area. All concentrations have been normalized to a flue gas content of 15% O_2 (dry basis). Flaming effective time periods are highlighted in gray. In the first combustion cycle the throttling valve of the wood stove was closed to 50% at t = 22–37 mins, resulting in choked combustion. In the second combustion batch no data is reported between t = 90–100 mins due to maintenance of the dilution system.

reduced flue gas temperatures lead to strongly increased intensity of markers of particle phase hydrocarbons ($^{27}C_2H_3^+$) and increased particle mass emission factors. Adverse combustion conditions were identified during start-up from cold stove, choked combustion with reduced air supply, and following the addition of fuel before efficient combustion was reestablished. During the burnout phase of each cycle, the CO emissions were increased while the influence on the particle emissions was less pronounced.

[30] Markers of volatilized ash compounds (such as $^{113}K_2Cl^+$) showed the opposite trend, typically increasing in relative intensity with increasing combustion temperature, for example, during flaming effective combustion. This is expected as the release of ash compounds from the fuel increases with increasing temperature, but is also caused by a decrease in the proportion of organics in the particles. The ratio of marker fragments for EC (sum of $^{24}C_2^-$, $^{36}C_3^-$, $^{48}C_4^-$) divided by the sum of the intensities of three marker fragments for OC ($^{41}C_2HO^-$, $^{42}CNO^-$, and $^{59}C_2H_3O_2^-$) also increased strongly with increasing temperature. The absolute intensity of the EC markers was strong (not shown) during flaming effective wood combustion at the lowest CO levels in this study (<200 ppm at 15% O_2, Figure 5). This shows that this type of wood stove is expected to emit EC during all combustion phases, in contrast to modern wood pellet burners which can emit below 1% of the particle mass as OC plus EC during optimized burn [*Londahl et al.*, 2008]. The vacuum aerodynamic size distribution as a function of time and phase in this experiment is given in Figure S3.

[31] TEOM data was only available for the first 45 min of the experiment reported in Figure 5, but generally the $PM_{1.5}$ mass concentration from the TEOM correlated well with the volume weighted (effective volume) SMPS concentration. The TEOM/SMPS concentration ratio increased by a factor of 2 during lower combustion temperatures, for example, the period with reduced air supply (choked) shown in Figure 5a. The EC to OC peak ratio was decreased during these periods of combustion at lower temperatures. We interpret this dependence on the combustion conditions to mean that most particles detected with the ATOFMS consist of a soot core throughout the experiment, but that the increased mass emissions during lower combustion temperatures are mainly caused by organic compounds which condense onto the soot agglomerates.

[32] Condensation of organics onto soot agglomerates causes an increased effective density and more compact particles [*Pagels et al.*, 2009]. The ratio of TEOM mass

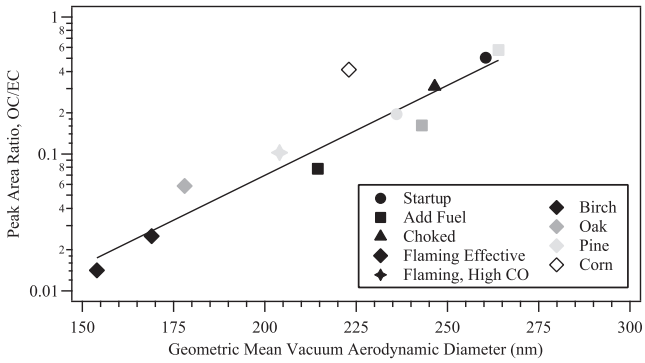

Figure 6. Relationship between the geometric mean diameter of the vacuum aerodynamic size distribution detected with ATOFMS and the ratio of major marker ions for organic and elemental carbon. Symbols indicate the combustion phase, and the intensity of gray indicates fuel, as shown in the legend. Corn combustion was omitted from the fit. The OC/EC peak ratio was determined using the sum of the intensities of three marker fragments for OC ($^{41}C_2HO^-$, $^{42}CNO^-$, and $^{59}C_2H_3O_2^-$) divided by the sum of three marker fragments for EC($^{24}C_2^-$, $^{36}C_3^-$, and $^{48}C_4^-$).

concentration to SMPS volume concentration can be viewed as a volume weighted average effective density, although differences in the sampled size range between the two instruments makes quantitative comparison with effective densities for soot sources given in the literature uncertain.

[33] We also found that the geometric mean diameter (GMD) of the vacuum aerodynamic (D_{va}) size distribution increases with increasing OC/EC marker ratio as shown in Figure 6. The smallest GMDs were found for flaming effective combustion (150–175 nm), for which the OC/EC ratio was very low. The low-temperature combustion phases that were associated with a higher OC/EC ratio (addition of fuel, start-up, and choked combustion) resulted in larger GMD (up to 260 nm). The increased coating thickness with increasing OC/EC is consistent with increased effective density and D_{va}.

[34] Average mass spectra for three different combustion phases/conditions are given in Figure S2. Trends in marker ions observed during start-up from cold stove, choked, and flaming effective combustion for the birch fuel are shown in Figure 7. Generally, hydrocarbon fragments, PAH fragments and fragments representing oxidized organics show the largest enhancements during start-up from a cold stove, while fragments containing both nitrogen and carbon show a stronger enhancement during choked combustion compared to start-up. It should be pointed out that many organic compounds (except PAHs) have low ionization efficiencies in the ATOFMS and may contribute significantly to the particle mass during these periods even though the relative intensity of these peaks is rather weak [*Gross et al*., 2006].

[35] The organic signatures during start-up (Figure S2) show similarities to that of pure levoglucosan [*Silva et al*., 1999], including strong peaks at m/z = -41, -59, -71, +27, +31 and +37). In the positive spectra there are also bands of organic markers at, for example, m/z = 48–51 and 60–63 that appear at start-up and to a lesser extent at choked combustion. *Weimer et al*. [2008] concluded that levoglucosan and related compounds were mainly emitted during the start-up phase, while strongly oxidized organics dominated during the burnout phase.

[36] PAHs show strong enhancements during start-up, while flaming effective shows stronger relative PAH intensity than choked. This suggests that PAHs show a different dependence on the combustion parameters than the marker fragments of hydrocarbon and oxidized organics. This is expected since PAHs have a much higher thermal stability than most other organic particle phase compounds. The dominant PAH peaks shift from markers of four-ring PAHs (m/z = 200–204, MW = 202) during start-up to markers of five-ring PAHs (m/z = 250–255, MW = 252) during flaming effective combustion. The results for the start-up phase are similar to ATOFMS results of combustion of eugenol

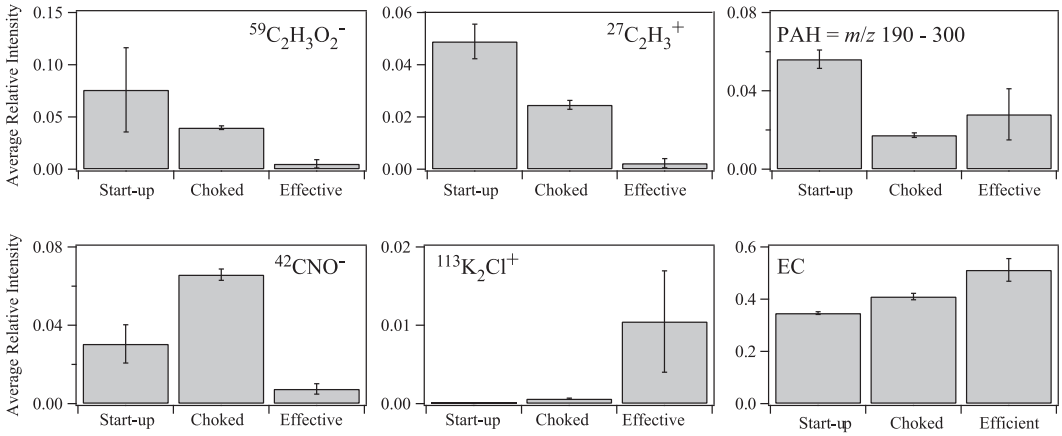

Figure 7. Trends in the average relative peak intensity of (top) markers for oxidized organics, hydrocarbons, and PAHs and (bottom) compounds containing both nitrogen and organics, potassium chloride, and EC as a function of combustion phase (start-up, choked, and flaming effective) in ATOFMS spectra, averaged over all fuels. Choked combustion was only studied for the birch fuel. Error bars represent ±1 standard deviation of replicate measurements.

[*Baeza-Romero et al*., 2010], a common pyrolysis product of lignin which was associated with four-ring PAHs (with $MW = 202$) such as fluoranthene and pyrene.

[37] The anticorrelation between markers of efficient combustion (e.g., K_2Cl^+) and the oxidized organic fragments (e.g., $m/z = -41, -59$) has implications for source-receptor methods that are based on either levoglucosan or potassium tracer techniques. These techniques will be sensitive to different aspects of biomass combustion emissions, with potassium being more sensitive to high-temperature complete combustion and levoglucosan being more sensitive to low-temperature smoldering combustion. Recently, *Harrison et al*. [2012] showed a strong variability of the levoglucosan to potassium ratio in measurements in several locations in the UK.

3.4. Single-Particle Mass Spectral Trends Based on Particle Composition

[38] In addition to analysis of marker ions, spectra were clustered using the *k*-means algorithm in Enchilada [*Gross et al*., 2010] to investigate temporal trends in the types of single-particle mass spectra observed in different combustion phases of each fuel, as described in the supporting

Table 1. Description of Particle Types From *k*-Means Clustering ($k = 6$) of Particles Emitted From Pine, Oak, Birch, and Corn Combustion[a]

	Fraction of Particles		Ions in Cluster Center						
ClusterName	Wood Fuel	Corn Fuel	Hydrocarbon	Elemental Carbon	PAHs	Sulfate ($^{97}HSO_4^-$)	Phosphate	K_xCl_y (x = 1, 2; y = 1, 2)	Other Significant Ions
Ash, soot, nitrate	0.327	0.441		–	+	–	–	±	$^{26}CN^-/C_2H_2^-$, $^{74}C_3H_6O_2^-$
Ash, soot	0.584	0.009	+	±		–		+	$^{26}CN^-/C_2H_2^-$
Hydrocarbon (HC)	0.054	0.156	+	±	+	–	–	-	$^{18}NH_4^+$
Ash, HC, nitrate	0.024	0.023	+	–	+	–		±	
Ash, phosphate	0.001	0.371		±		–	–	±	
PAH	0.011	0.000		–	+	–		±	$^{125}H(NO_3)_2^-$

[a]The polarity of an ion is indicated if the ion is observed in a cluster center. All cluster centers contain $^{39}K^+$ and $^{46}NO_2^-$ ions. See Figure S4 for spectra of the cluster centers. The fraction of particles is calculated over the whole experiment, including all combustion phases, from startup to burnout.

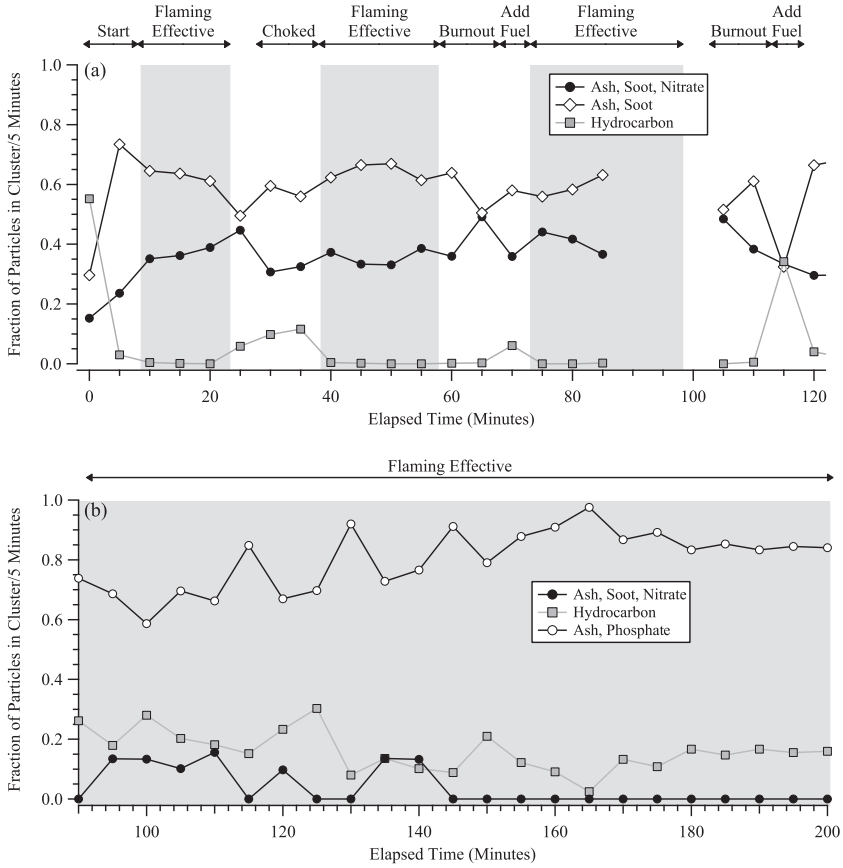

Figure 8. Temporal variation of the fraction of particles in each cluster center for selected periods within the (a) birch and (b) corn experiments. Only clusters containing more than 5% of the particles in any 5 min time bin are shown. Flaming effective time periods are highlighted in gray.

information. Trends in the complete mass spectra, in contrast to marker ions alone, make it possible to generalize from the data obtained in controlled studies like these to particle types which might be observed during ambient measurements. The fraction of the total observed particles assigned to each cluster, and the most abundant ions in the clusters, are summarized in Table 1. Temporal profiles of the significant clusters observed in birch and corn combustion experiments are shown in Figure 8; birch temporal profiles are similar to those observed for the pine and oak fuels, as well. Cluster center spectra, which represent an average spectrum of all particles assigned to the cluster are shown in Figure S4. The most populous cluster from the three wood fuels ("ash, soot") has a mass spectrum containing potassium chloride, elemental carbon, nitrate, and sulfate ions. Very few hydrocarbon ions and no PAHs are observed in this cluster. This particle type constitutes less than 0.1% of the particles observed during corn combustion, and thus this particle type can be seen as indicative of wood combustion.

[39] The second most populous cluster ("ash, soot, nitrates") showed a similar cluster center but with stronger nitrate and PAH signals. The temporal profile shows that the summed fraction of these two clusters decreases during start-up, when fuel is added, and during the choked combustion, consistent with a significantly different particle type present under these conditions.

[40] In experiments with each of the fuels (wood and corn), a "hydrocarbon" cluster that contains hydrocarbon ions as well as signatures from nitrates, sulfates, PAHs, and EC is present at times when combustion is inefficient. This cluster has the same temporal profile as CO, the SMPS volume concentration, the TEOM mass concentration, and the ATOFMS hydrocarbon marker ion $^{27}C_2H_3^+$ shown in Figure 5a. Essentially no particles of this type are observed during flaming effective wood combustion, suggesting that this particle type is a reliable marker for inefficient low-temperature combustion of biofuels.

[41] During corn combustion, the predominant particle types emitted differ from those seen during wood combustion (Figure 8), consistent with the results obtained by examining marker ions. Throughout the majority of the continuous flaming effective combustion in the corn experiment, 75 % of the particles observed were assigned to the "ash, phosphate" cluster center. During wood combustion this type of particle never made up more than 1.3% of the particles observed in any 5 min time period. This particle type is dominated by phosphate ions in the negative spectrum (consistent with the average relative ion intensity obtained from the corn combustion shown in Figure 4). It contains potassium and potassium chloride in the positive spectrum and sulfate and EC markers in the negative spectra. It does not contain PAHs and the hydrocarbon fragments are weak.

3.5. Size-Resolved Analysis of Marker Ions in Single-Particle Mass Spectra

[42] Figure 9a shows the vacuum aerodynamic size distribution of the full combustion cycle for birch and for the choked and flaming effective combustion phases. The GMD was 153 nm for flaming effective and 248 nm for choked combustion. The distribution of the full combustion cycle (including the period with choked combustion) has an intermediate GMD (197 nm) and is substantially wider.

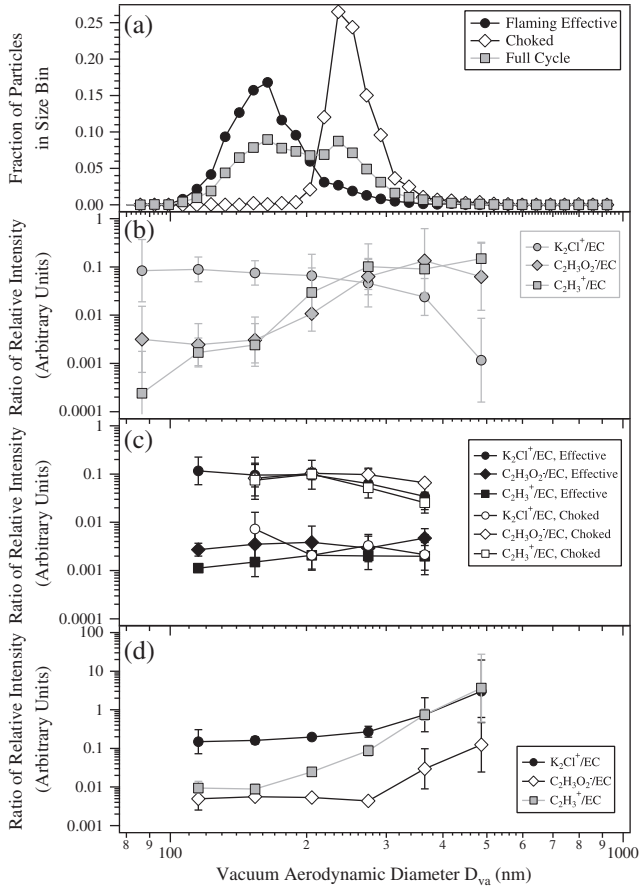

Figure 9. Size-resolved ratios of fragments observed in the mass spectra representing alkali salts ($^{113}K_2Cl^+$), oxidized organics ($^{59}C_2H_3O_2^-$), and hydrocarbons ($^{27}C_2H_3^+$) compared to EC (sum of $^{24}C_2^-$, $^{36}C_3^-$, and $^{48}C_4^-$). (a) Data are compared to the vacuum aerodynamic size distribution of particles for choked; flaming effective; and the full combustion cycle for the birch fuel, and data are reported for (b) birch combustion over the whole combustion cycle, (c) birch combustion during periods in the flaming phase with the vent fully open (flaming effective) and vent 50% closed (choked), and (d) flaming effective combustion for corn fuel. The $^{113}K_2Cl^+$/EC ratio has been multiplied by a factor of 5 in Figures 9b and 9c to ease visualization.

[43] Figure 9b shows size-resolved ratios between selected marker fragments representing potassium chloride ($^{113}K_2Cl^+$), oxidized organics ($^{59}C_2H_3O_2^-$) and hydrocarbons ($^{27}C_2H_3^+$) compared to elemental carbon (sum of $^{24}C_2^-$, $^{36}C_3^-$, $^{48}C_4^-$) for the full cycle in birch combustion. It was found that the relative intensity of these markers varies strongly as a function of D_{va}. The relative intensity of the potassium chloride fragment decreases relative to soot fragments with increasing D_{va}. An opposite and even stronger trend is found for marker fragments of both hydrocarbons and oxidized organics. As described above, a similar shift in composition arises when comparing the size integrated signatures of periods of effective burn with periods representing start-up and choked combustion.

[44] The size-dependent composition was also investigated separately for flaming effective and choked birch combustion

(Figure 9c). The size-dependent variations in signatures were much weaker in this case. This shows that the strongly size-dependent signatures found when averaging over the full combustion cycle were largely caused by significant differences in composition and size distributions between different combustion conditions/phases. In the signatures from the full cycle, the smaller particles emitted during flaming effective combustion give the main contribution below 200 nm and the larger particles emitted during start-up and choked combustion dominates above 200 nm.

[45] The stable flaming effective conditions during corn combustion, on the other hand, showed variations in chemical signatures as a function of particle size (Figure 9d). With increasing D_{va}, markers for oxidized organics and hydrocarbons showed strong increases in relative intensity compared to markers of EC, while for alkali salts the increase compared to EC was weaker. This is consistent with agglomerated soot particles predominantly being present in smaller aerodynamic sizes, due to their low effective density [*Park et al*., 2008]. As combustion products cool, alkali salts begin to condense first on the soot agglomerates, while the organics condense later at lower temperature. The fraction of corn emission particles sized by the ATOFMS, but which did not generate mass spectra, increased strongly with increasing D_{va}; such trends were much weaker for the wood fuels.

3.6. Measurements of Individual Mobility-Classified Particles

[46] In a few experiments with the corn stove, a differential mobility analyzer was used upstream of the ATOFMS. The aerodynamic sizes and chemical signatures of individual mobility classified particles were then determined with the ATOFMS. This enabled the separation of different particle types at a given mobility size (D_{me}) by effective density (ρ_{eff}), as defined from measurements of D_{me} and D_{va} [*DeCarlo et al*., 2004]. The effective density defined in this way is given in equation (1), where ρ_0 is the density of water.

$$\rho_{eff} = \frac{D_{va}}{D_{me}}\rho_0 \quad (1)$$

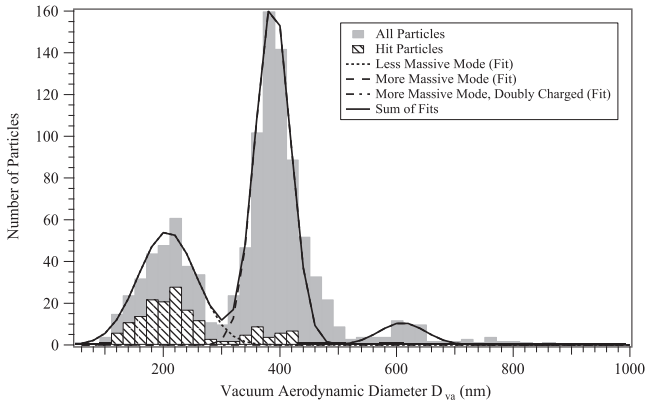

Figure 10. Vacuum aerodynamic size distribution for hit and total particles measured with the ATOFMS from the corn stove. The ATOFMS sampled 200 nm mobility-classified particles. The data show evidence of an external mixture. Normal Gaussian distributions were fit to the data.

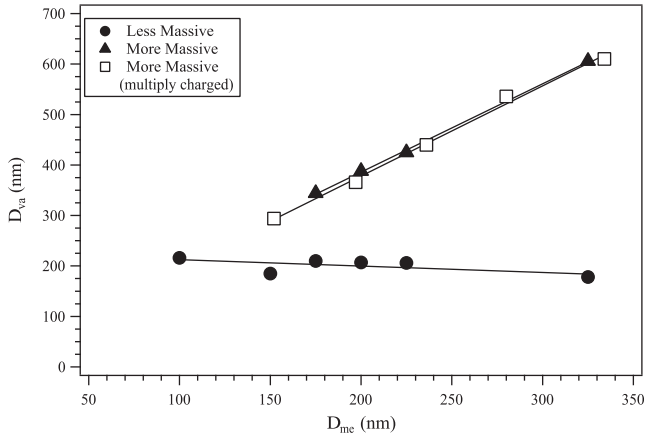

Figure 11. Relationship between mobility diameter (D_{me}) and vacuum aerodynamic diameter (D_{va}) for the different particle classes shown in Figure 10 for the corn particle emissions. The particles generated mass spectra from approximately 50% and 5% of the less and more massive particles, respectively. For multiply-charged more massive particles, D_{me} is plotted at the larger mobility size the particle would have if it was singly charged.

[47] Particle vacuum aerodynamic size distributions were typically bimodal or trimodal for mobility-classified particles with mobility diameters of 100, 150, 175, 200, 225 and 325 nm. This is illustrated for the 200 nm mobility size particles in Figure 10. Less massive particles of $D_{va} \sim 210$ nm (GMD), which generated mass spectra ~50% of the time, made up one mode. These particles were dominated by the ash-related compounds overlaid on distinct EC signatures. An effective density of about 1 g/cm^3 was found at $D_{me} = 200$ nm (equation (1)). This is substantially higher than for diesel soot [*Park et al*., 2003] but is consistent with soot agglomerates with a substantial coating of inorganic ash material (such as potassium phosphate, potassium sulfate and potassium chloride) and organics [*Pagels et al*., 2009].

[48] It is important to note that these particles had a vacuum aerodynamic size essentially independent of mobility size, shown in Figure 11, as has been found previously for other types of soot agglomerates [*Slowik et al*., 2004; *Park et al*., 2008; *Schneider et al*., 2006]. That these less massive soot particles have a vacuum aerodynamic size distribution in the range 150–250 nm is consistent with the ATOFMS measurements on polydisperse corn emissions in Figure 9d, where markers for elemental carbon are enriched in the size range <300 nm.

[49] When comparing with the D_{va} size distribution of particles that generated valid mass spectra for the corn emissions without mobility classification upstream the ATOFMS, one finds that the GMD is similar (220 nm). Further, the geometric standard deviation (GSD) of the D_{va} distribution is also similar when selecting one mobility diameter and when selecting the full size distribution (~1.25 in both cases). This is an expected result from Figure 11, as soot agglomerates of a wide range of mobility sizes all have essentially the same D_{va}.

[50] In contrast, the more massive particle mode showed linearly increasing D_{va} with increasing D_{me}, as seen in Figure 11. At the smaller mobility sizes a peak at even larger

D_{va} was found, which consisted of multiply charged particles transmitted by the DMA at each DMA voltage. Experimental data for both singly and multiply charged particles agrees well with a linear fit to the D_{va} versus D_{me} relationship. The fit suggests that these particles are near spherical with an effective density of 1.8 ± 0.1 g/cm^3, independent of size over the mobility size range 150–325 nm.

[51] Very few (~5%) of these more massive particles produced valid mass spectra. The few detected mass spectra showed the presence of alkali containing compounds, which are typically easy to ionize in the ATOFMS. It could be that the alkali components are hidden inside an organic coating which would decrease the ionization probability. It could also be that the few particles which did generate a mass spectrum may not have been representative of all of the larger particles generated in these experiments.

[52] Organic particles (for example, formed by smoldering corn kernels at lower temperature some distance away from the main combustion zone) may have a low ionization probability but most oxidized organic compounds have a density slightly lower (in the range of 1.3–1.7 g/cm^3) than that detected in these experiments. For example, pure levoglucosan has a density of 1.69 g/cm^3. Several organic markers from corn also contained nitrogen (m/z = -26, -42) and thus nitrogen-containing organics may be an important class of compounds emitted during corn combustion. The exact nature and density of these compounds is not known.

[53] There was much weaker size dependence for the probability of generating mass spectra in the wood stove experiments, indicating that the class of difficult-to-ionize particles was specific for the corn stove. The polydisperse wood stove emissions also showed very narrow D_{va} size distributions (Figure 9a) with GSD = ~1.1 for choked combustion and ~1.2 for flaming effective combustion. This is consistent with a similar relationship between D_{va} and D_{me} for the wood combustion emissions as that for the less massive corn emission particles at each well-defined combustion phase. However, over the full combustion cycle the GSD was significantly larger (~1.4).

4. Summary and Conclusions

[54] We have investigated the variations in chemical signatures of single particles as a function of combustion phase, fuel and vacuum aerodynamic size in emissions from a modern wood stove and a corn stove. The strongest variations were found for organic marker ions when comparing different combustion phases. The organic marker ions, which to some extent resembled that of pure levoglucosan particles, were correlated with increased PM and CO emission factors, decreased flue gas temperatures, and the prevalence of a single-particle type with strong organic marker fragments. This indicates that a large fraction of the increase in mass emission factor during start-up from cold stove, addition of fuel, and reduced air supply is due to organic components.

[55] During flaming combustion at low CO emissions in both the wood stove and the corn stove, the organic signatures were strongly reduced and the mass spectra were dominated by potassium, chloride, sulfate and nitrate fragments overlaid on distinct soot patterns. Major differences between corn and wood stove emissions were the presence of strong phosphate fragments and a smaller fraction of markers of oxidized organics for the corn emissions. For the wood stove, the chemical signatures of the emissions varied strongly over size when averaging over the full combustion cycle, while they were essentially independent of size for well-defined combustion phases. Thus, the variation in size-dependent composition over a full batch is a result of changes in both size distribution and chemistry between combustion phases.

[56] Vacuum aerodynamic size distributions and ion fragments of mobility-classified corn emissions were consistent with particles being composed of soot agglomerates with condensed organic and ash species (such as potassium chloride, sulfates and phosphates). A second particle type, consistent with near spherical particles, was identified. This particle type had a low ionization probability in the ATOFMS and was hypothesized to consist of organics. Distinctly different particle types dominated for wood and corn stove emissions, which can be used to apportion particles in ambient air to emissions from wood stove and crop fuel combustion.

[57] To reduce smoke emissions from wood stoves, extended low-temperature combustion such as choked combustion with reduced air supply should be avoided. This strongly reduces the emissions of most organics with exceptions of thermally stable organic compounds such as polycyclic aromatic hydrocarbons (PAHs) for which the emission situation is more complex and requires further study.

[58] Smoke emissions can also be reduced by replacing modern wood stoves with pellet stoves that allow more controlled air and fuel supply and mixing, and thus a more complete combustion. Examples are wood pellet stoves and corn stoves of the type described here.

[59] **Acknowledgments.** J.P. was supported by the Swedish Research Council FORMAS, grants 2005-1515 and 2010-1678, and the ERA-NET Project Biohealth. D.G. was supported with a Bush Fellowship Faculty Development Grant from Carleton College. UMN researchers were supported by NSF grant NSF/ATM-0096555. Patience and help from Woodland Stoves, Minneapolis, are warmly acknowledged. We thank TSI, Inc., for the loan of the CaCalc model 7315 flue gas analyzer and David Kittelson for loaning us the ECOM flue gas analyzer. Christoffer Boman (Umeå University, Sweden) is greatly acknowledged for giving feedback on an early version of the paper.

References

Alfarra, M. R., A. S. H. Prevot, S. Szidat, J. Sandradewi, S. Weimer, V. A. Lanz, D. Schreiber, M. Mohr, and U. Baltensperger (2007), Identification of the mass spectral signature of organic aerosols from wood burning emissions, *Environ. Sci. Technol.*, *41*(16), 5770–5777.

Baeza-Romero, M. T., J. M. Wilson, E. M. Fitzpatrick, J. M. Jones, and A. Williams (2010), In situ study of soot from the combustion of a biomass pyrolysis intermediate-eugenol-and n-decane using aerosol time of flight mass spectrometry, *Energy Fuel*, *24*, 439–445.

Bolling, A. K., J. Pagels, K. E. Yttri, L. Barregard, G. Sallsten, P. E. Schwarze, and C. Boman (2009), Health effects of residential wood smoke particles: The importance of combustion conditions and physicochemical particle properties, *Particle Fibre Toxicol.*, *6*:*29*, doi:10.1186/1743-8977-6-29.

Boman, C., A. Nordin, D. Bostrom, and M. Ohman (2004), Characterization of inorganic particulate matter from residential combustion of pelletized biomass fuels, *Energy Fuel*, *18*(2), 338–348.

Boström, D., N. Skoglund, A. Grimm, C. Boman, M. Ohman, M. Brostrom, and R. Backman (2012), Ash transformation chemistry during combustion of biomass, *Energy Fuel*, *26*, 85–93.

Caseiro, A., H. Bauer, C. Schmidl, A. P. Casimiro, and H. Puxbaum (2009), Wood burning impact on PM10 in three Austrian regions, *Atmos. Env.*, *43*, 2186–2195.

Christensen, K. A., M. Stenholm, and H. Livbjerg (1998), The formation of submicron aerosol particles, HCl and SO_2 in straw-fired boilers, *J. Aerosol Sci.*, *29*(4), 421–444.

DeCarlo, P. F., J. G. Slowik, D. R. Worsnop, P. Davidovits, and J. L. Jimenez (2004), Particle morphology and density characterization by combined mobility and aerodynamic diameter measurements. Part 1: Theory, *Aerosol Sci. Technol.*, *38*, 1185–1205.

Dutcher, D. D., et al. (2011), Emissions from soy biodiesel blends: A single particle perspective, *Atmos. Environ.*, *45*(20), 3406–3413.

Favez, O., H. Cachier, J. Sciare, R. Sarda-Estève, and L. Martinon (2009), Evidence for a significant contribution of wood burning aerosols to PM2. 5 during the winter season in Paris, France, *Atmos. Env.*, *43*, 3640–3644.

Fine, P. M., G. R. Cass, and B. R. T. Simoneit (2004), Chemical characterization of fine particle emissions from the wood stove combustion of prevalent United States tree species, *Environ. Eng. Sci.*, *21*(6), 705–721.

Gard, E., J. E. Mayer, B. D. Morrical, T. Dienes, D. P. Fergenson, and K. A. Prather (1997), Real-time analysis of individual atmospheric aerosol particles: Design and performance of a portable ATOFMS, *Anal. Chem.*, *69*(20), 4083–4091.

Grieshop, A. P., J. M. Logue, N. M. Donahue, and A. L. Robinson (2009), Laboratory investigation of photochemical oxidation of organic aerosol from wood fires, 1: Measurement and simulation of organic aerosol evolution, *Atmos. Chem. Phys.*, *9*(4), 1263–1277.

Gross, D. S., et al. (2006), Real-time measurement of oligomeric species in secondary organic aerosol with the aerosol time-of-flight mass spectrometer, *Anal. Chem.*, *78*(7), 2130–2137.

Gross, D. S., et al. (2010), Environmental chemistry through intelligent atmospheric data analysis, *Environ. Modell. Software*, *25*(6), 760–769.

Harrison, R., M. D. C. S. Beddows, L. Hu, and J. Yin (2012), Comparison of methods for evaluation of wood smoke and estimation of UK ambient concentrations, *Atmos. Chem. Phys. Discuss.*, *12*, 6805–6838.

Healy, R. M., S. Hellebust, I. Kourtchev, A. Allanic, I. P. O'Connor, J. M. Bell, D. A. Healy, J. R. Sodeau, and J. C. Wenger (2010), Source apportionment of PM(2.5) in Cork Harbour, Ireland using a combination of single particle mass spectrometry and quantitative semi-continuous measurements, *Atmos. Chem. Phys.*, *10*(19), 9593–9613.

Heringa, M. F., P. F. DeCarlo, R. Chirico, T. Tritscher, J. Dommen, E. Weingartner, R. Richter, G. Wehrle, A. S. H. Prevot, and U. Baltensperger (2011), Investigations of primary and secondary particulate matter of different wood combustion appliances with a high-resolution time-of-flight aerosol mass spectrometer, *Atmos. Chem. Phys.*, *11*(12), 5945–5957.

Intergovernmental Panel on Climate Change (2007), Climate Change 2007: The Physical Science Basis. Contribution of Working Group I to the Fourth Assessment Report of the Intergovernmental Panel on Climate Change, edited by S. Solomon et al. Cambridge Univ. Press, Cambridge, U. K.

Johansson, L. S., B. Leckner, L. Gustavsson, D. Cooper, C. Tullin, and A. Potter (2004), Emission characteristics of modern and old-type residential boilers fired with wood logs and wood pellets, *Atmos. Environ.*, *38*(25), 4183–4195.

Lillieblad, L., A. Szpila, M. Strand, J. Pagels, K. Rupar-Gadd, A. Gudmundsson, E. Swietlicki, M. Bohgard, and M. Sanati (2004), Boiler operation influence on the emissions of submicrometer-sized particles and polycyclic aromatic hydrocarbons from biomass-fired grate boilers, *Energy Fuel*, *18*(2), 410–417.

Londahl, J., J. Pagels, C. Boman, E. Swietlicki, A. Massling, J. Rissler, A. Blomberg, M. Bohgard, and T. Sandstrom (2008), Deposition of biomass combustion aerosol particles in the human respiratory tract, *Inhalation Toxicol.*, *20*(10), 923–933.

McGuire, M. L., et al. (2011), Elucidating determinants of aerosol composition through particle-type-based receptor modeling, *Atmos. Chem. Phys.*, *11*(15), 8133–8155.

Moffet, R. C., B. de Foy, L. T. Molina, M. J. Molina, and K. A. Prather (2008), Measurement of ambient aerosols in northern Mexico City by single particle mass spectrometry, *Atmos. Chem. Phys.*, *8*(16), 4499–4516.

Naeher, L. P., M. Brauer, M. Lipsett, J. T. Zelikoff, C. D. Simpson, J. Q. Koenig, and K. R. Smith (2007), Woodsmoke health effects: A review, *Inhalation Toxicol.*, *19*(1), 67–106.

Pagels, J., A. F. Khalizov, P. H. McMurry, and R. Y. Zhang (2009), Processing of soot by controlled sulphuric acid and water condensation mass and mobility relationship, *Aerosol Sci. Technol.*, *43*(7), 629–640.

Pagels, J., M. Strand, J. Rissler, A. Szpila, A. Gudmundsson, M. Bohgard, L. Lillieblad, M. Sanati, and E. Swietlicki (2003), Characteristics of aerosol particles formed during grate combustion of moist forest residue, *J. Aerosol Sci.*, *34*(8), 1043–1059.

Park, K., F. Cao, D. B. Kittelson, and P. H. McMurry (2003), Relationship Between Particle Mass and Mobility for Diesel Exhaust Particles, *Environ. Sci. Technol.*, *37*, 577–583.

Park, K., et al. (2008), Tandem measurements of aerosol properties—A review of mobility techniques with extensions, *Aerosol Sci. Technol.*, *42*(10), 801–816.

Pettersson, E., C. Boman, R. Westerholm, D. Bostrom, and A. Nordin (2011), Stove performance and emission characteristics in residential wood log and pellet combustion, part 2: Wood stove, *Energy Fuel*, *25*, 315–323.

Pratt, K. A., and K. A. Prather (2012), Mass spectrometry of atmospheric aerosols—Recent developments and applications. Part II: On-line mass spectrometry techniques, *Mass Spectrom. Rev.*, *31*, 17–48.

Qin, X. Y., and K. A. Prather (2006), Impact of biomass emissions on particle chemistry during the California Regional Particulate Air Quality Study, *Int. J. Mass Spectrom.*, *258*(1–3), 142–150.

Rissler, J., J. Pagels, E. Swietlicki, A. Wierzbicka, M. Strand, L. Lillieblad, M. Sanati, and M. Bohgard (2005), Hygroscopic behavior of aerosol particles emitted from biomass fired grate boilers, *Aerosol Sci. Technol.*, *39*(10), 919–930.

Schneider, J., S. Weimer, F. Drewnick, S. Borrmann, G. Helas, P. Gwaze, O. Schmid, M. O. Andreae, and U. Kirchner (2006), Mass spectrometric analysis and aerodynamic properties of various types of combustion-related aerosol particles, *Int. J. Mass Spectrom.*, *258*, 37–49.

Sehlstedt, M., et al. (2010), Antioxidant airway responses following experimental exposure to wood smoke in man, *Particle Fibre Toxicol.*, *7*:*21*.

Silva, P. J., D. Y. Liu, C. A. Noble, and K. A. Prather (1999), Size and chemical characterization of individual particles resulting from biomass burning of local Southern California species, *Environ. Sci. Technol.*, *33* (18), 3068–3076.

Slowik, J. G., K. Stainken, P. Davidovits, L. R. Williams, J. T. Jayne, C. E. Kolb, D. R. Worsnop, Y. Rudich, P. F. DeCarlo, and J. L. Jimenez (2004), Particle morphology and density characterization by combined mobility and aerodynamic diameter measurements. Part 2: Application to combustion-generated soot aerosols as a function of fuel equivalence ratio, *Aerosol Sci. Technol.*, *38*(12), 1206–1222.

Tao, G., P. Geladi, T. A. Lestander, and S. Xionga (2012), Biomass properties in association with plant species and assortments. II: A synthesis based on literature data for ash elements, *Renewable Sustainable Energy Rev.*, *16*, 3507–3522.

Tissari, J., O. Sippula, J. Kouki, K. Vuorio, and J. Jokiniemi (2008a), Fine particle and gas emissions from the combustion of agricultural fuels fired in a 20 kW burner, *Energy Fuel*, *22*(3), 2033–2042.

Tissari, J., K. Hytonen, O. Sippula, and J. Jokiniemi (2009), The effects of operating conditions on emissions from masonry heaters and sauna stoves, *Biomass Bioenergy*, *33*(3), 513–520.

Tissari, J., et al. (2008b), Fine particle and gaseous emissions from normal and smouldering wood combustion in a conventional masonry heater, *Atmos. Environ.*, *42*(34), 7862–7873.

van Loo, S., and J. Koppejan (Eds.) (2008), *The Handbook of Biomass Combustion and Co-firing*, Earthscan, London.

Weimer, S., M. R. Alfarra, D. Schreiber, M. Mohr, A. S. H. Prevot, and U. Baltensperger (2008), Organic aerosol mass spectral signatures from wood-burning emissions: Influence of burning conditions and wood type, *J. Geophys. Res.*, *113*, D10304, doi:10.1029/2007JD009309.

Wierzbicka, A., L. Lillieblad, J. Pagels, M. Strand, A. Gudmundsson, A. Gharibi, E. Swietlicki, M. Sanati, and M. Bohgard (2005), Particle emissions from district heating units operating on three commonly used biofuels, *Atmos. Environ.*, *39*(1), 139–150.

Wiinikka, H., R. Gebart, C. Boman, D. Bostrom, and M. Ohman (2007), Influence of fuel ash composition on high temperature aerosol formation in fixed bed combustion of woody biomass pellets, *Fuel*, *86*(1–2), 181–193.

Wolnik, K. A., F. L. Fricke, S. G. Capar, M. W. Meyer, R. D. Satzger, E. Bonnin, and C. M. Gasgon (1985), Elements in major raw agricultural crops in the United States. 3. Cadmium, lead and eleven other elements in carrots, field corn, onions, rice, spinach, and tomatoes, *J. Agric. Food Chem.*, *33*, 807–811.